Enhancement of nanovoid formation in annealed amorphous Al_20_3 including W

doi: 10.1063/1.3639290

Enhancement of nanovoid formation in annealed amorphous Al_2O_3 including W

R. Nakamura,[1,a)] M. Ishimaru,[1] A. Hirata,[2] K. Sato,[3] M. Tane,[1] H. Kimizuka,[4] T. Shudo,[1] T. J. Konno,[3] and H. Nakajima[1]
[1]*The Institute of Scientific and Industrial Research, Osaka University, Mihogaoka 8-1, Ibaraki, Osaka 567-0047, Japan*
[2]*World Premier International Research Center, Advanced Institute for Materials Research, Tohoku University, Katahira 2-1-1, Sendai 980-8577, Japan*
[3]*Institute for Materials Research, Tohoku University, Katahira 2-1-1, Sendai 980-8577, Japan*
[4]*Graduate School of Engineering Science, Osaka University, Toyonaka, Osaka 560-8531, Japan*

(Received 20 June 2011; accepted 11 August 2011; published online 27 September 2011)

The effect of W on the nanovoid formation in annealed amorphous Al_2O_3 was studied by transmission electron microscopy and molecular dynamics simulations. A comparison of the void formation behavior in electron-beam deposited Al_2O_3 (without W) and resistance-heating deposited Al_2O_3 (with 10 at. % W) revealed that W enhances the formation and growth of nanovoids. An analysis of the pair distribution function (PDF) in both types of amorphous Al_2O_3 showed that the introduction of W into amorphous Al_2O_3 brings about a significant change in the amorphous structure. Furthermore, it was found by high-angle annular dark-field scanning transmission electron microscopy (HAADF-STEM) that sub-nm sized W clusters exist in as-deposited Al_2O_3 prepared by resistance-heating and then dissolve in the amorphous matrix with annealing. The combination of PDF analysis and HAADF-STEM observation provides evidence that the enhancement of void formation originates in the heterogeneous short-range atomic configurations induced by the addition of W. © *2011 American Institute of Physics*. [doi:10.1063/1.3639290]

I. INTRODUCTION

Nanoporous oxides have attracted extensive attention as functional materials in categories such as ion exchange, molecular separation, catalysis, chromatography, and energy storage, because the large surface-to-volume ratio is expected to improve these characteristics.[1,2]

A number of methods have been proposed to fabricate different types of nanoporous metal-oxides, including Al_2O_3, TiO_2, ZrO_2, WO_3, and SnO_2.[3] Nanoporous oxides are usually fabricated by chemical synthesis routes, which combine the use of a template and an etching process. The chemical synthesis techniques are based on the concept of creating spaces by eliminating the nano-sized templates. In our research, however, a bottom-up technique of producing nanoporous structures through the accumulation of atomic level spaces is employed. Amorphous Al_2O_3 (Refs. 4 and 5) and WO_3 (Ref. 4) were found to become nanoporous structures as a result of annealing in air. The evolution of nanovoids can be explained by the accumulation of the free volume in amorphous Al_2O_3 and WO_3, both of which have 20–30% lower density than their crystalline phases.[6–8]

As explained in earlier papers,[4,5] void formation takes place in the amorphous states before crystallization. The experimental and theoretical analyses carried out by Tane *et al.*[5] indicated that as-deposited amorphous Al_2O_3 consists of lower- and higher-density regions containing lower and higher fractions of AlO_6 basic units, respectively, and that local density growth in the unstable lower-density regions during annealing leads to nanovoid formation before crystallization. Because their results suggest that void formation behavior is related closely to the changes in amorphous structure, the effect of changes in amorphous structure on the void formation behavior in Al_2O_3 needs to be elucidated. One of the ideas for inducing structural changes is to add a third element, which can bring about changes in both the microstructure and the kinetic processes toward crystallization. Investigating the effect of this third element on nanovoid formation can lead to a better understanding of how to control the size and density of nanovoids, which is important from a scientific perspective and also in terms of the potential applications of these materials.

In this study, the focus was on the void formation behavior of amorphous Al_2O_3 prepared by the resistive heating (RH) technique using a W coil, because W was inevitably introduced in the self-evaporation process from the W basket heating source. The effect of W on the void formation in amorphous Al_2O_3 was determined by comparing the void formation behavior and radial distribution function of annealed amorphous RH-Al_2O_3 with W to those of Al_2O_3 without W prepared by electron-beam (EB) evaporation. The pair distribution function of amorphous Al_2O_3 was also analyzed by molecular dynamics (MD) simulations. In addition, high-angle annular dark-field scanning transmission electron microscopy (HAADF-STEM) was used in order to observe the distribution of W in RH-Al_2O_3 because this technique provides a clear contrast between heavy atoms in matrices.

[a)]Author to whom correspondence should be addressed. Electronic mail: rnakamur@sanken.osaka-u.ac.jp.

II. EXPERIMENTAL PROCEDURES

Thin films of amorphous Al_2O_3 were prepared both by electron-beam (EB) and resistive heating (RH) deposition techniques in a high-vacuum chamber. A high-purity tablet and a grain of Al_2O_3 (99.99%) were used as the evaporation source for the EB and RH deposition, respectively. For the RH deposition, a W coil was used as the heating source. A cleavage NaCl crystal was used as the substrate, and the substrate at deposition was at ambient temperature. The NaCl on which the 15~20 nm thick oxide thin film was deposited was put into distilled water, and then the floating thin film was mounted onto a Pt grid. The amorphous oxides on the Pt grid were subjected to heat-treatment in an electric furnace in air at 873~1073 K for 3.6 ks. The changes in morphology and structure were examined by a Hitachi H-800 type TEM operated at 200 kV and FEI Titan 80-300 TEM operated at 300 kV. The latter was equipped with a high-angle annular dark-field (HAADF) detector. The selected-area electron diffraction (SAED) patterns of the as-deposited and annealed thin films were taken by a JEOL JEM-3000F type TEM at 100 K using a cooling holder in order to avoid contamination. The intensities of the electron diffraction patterns recorded on an imaging plate (Eu^{2+} doped BaFBr) were analyzed quantitatively using a Digital Micro-Luminography FDL5000.[9,10] The composition was analyzed by a JEOL-3000F type TEM equipped with an energy dispersive X-ray spectroscope (EDS).

III. SIMULATION PROCEDURES

As previously reported, equilibrium MD simulations of amorphous Al_2O_3 were performed to enable the relationship between changes in atomic structure and density to be described.[5] On the basis of the same model, the atomistic structures of amorphous and liquid Al_2O_3 were analyzed to determine the heterogeneity of the structures. The Nosé-Hoover[11] and the Parrinello-Rahman[12] isobaric-isothermal thermostat and a Born-Mayer-Huggins-type pairwise potential with long-range Coulomb interaction (Matsui's potential[13]) were employed for the equilibrium MD simulations. The MD simulations were carried out in a hexagonal 2160 atoms supercell (consisting of $6 \times 6 \times 2$ unit cells of α-Al_2O_3) with the periodic boundary conditions imposed in all directions. First, the atoms were placed on the positions of an experimentally determined α-Al_2O_3 lattice.[14] Then, the temperature of the system was continuously increased from 300 to 3000 K at a rate of 10 K/ps under zero external stress, after which the system was equilibrated for 80 ps. A liquid Al_2O_3 model was obtained after cooling from 3000 to 2600 K at a rate of 0.1 K/ps and then equilibrating at 2600 K for 80 ps. An amorphous Al_2O_3 model was obtained at 300 K by cooling the liquid Al_2O_3 at 3000 K at a rate of 0.1 K/ps. The integration time step in all the MD simulations was 2 fs. For the prepared liquid and amorphous Al_2O_3 models, the total PDFs were analyzed. The PDF was also obtained for an amorphous Al_2O_3 model at 700 K after the temperature was raised from 300 to 700 K at a rate of 0.1 K/ps.

HAADF-STEM simulations were carried out for four structure models using STEM FOR WIN HREM code software (HREM Research Inc.). The four structure models for amorphous Al_2O_3 were as follows: (a) pure Al_2O_3 with a flat surface, (b) Al_2O_3 including a nano-pillar, (c) Al_2O_3 including a W cluster, and (d) Al_2O_3 with homogeneous W distribution following experimental results. The first step involved constructing a large model (10 056 atoms) with a dimension of $2.439 \times 3.443 \times 12.34$ nm^3 by combining 16 small orthogonal subcells (629 atoms), each of which was cut out from the amorphous Al_2O_3 systems (2160 atoms) obtained from MD simulations. Then a small Al_2O_3 pillar with a length of 12.34 nm was attached to the upper center part of the normal model for the second model. To construct the third model, a hole with a radius of 1.5 nm at the center part of the normal model was made and then the same-sized W clusters were embedded in the matrix. As for the fourth model, 878 Al atoms were replaced by W atoms in a random manner. A probe convergence angle of 10 mrad was used in the calculations, and the HAADF detector inner and outer angles were, respectively, 60 and 210 mrad.

IV. RESULTS AND DISCUSSION

Figure 1 shows the EDS spectra for as-deposited amorphous (a) EB-Al_2O_3 and (b) RH-Al_2O_3. As shown in Fig. 1(a), EB-Al_2O_3 is composed of aluminum and oxygen. The characteristic x-ray peaks for Pt originate from a Pt grid. In addition to Al and O, however, RH-Al_2O_3 includes W at a concentration of approximately 10 at. %. The deposition of W into amorphous Al_2O_3 can be attributed to the evaporation from the W coil used as a heating source for resistive

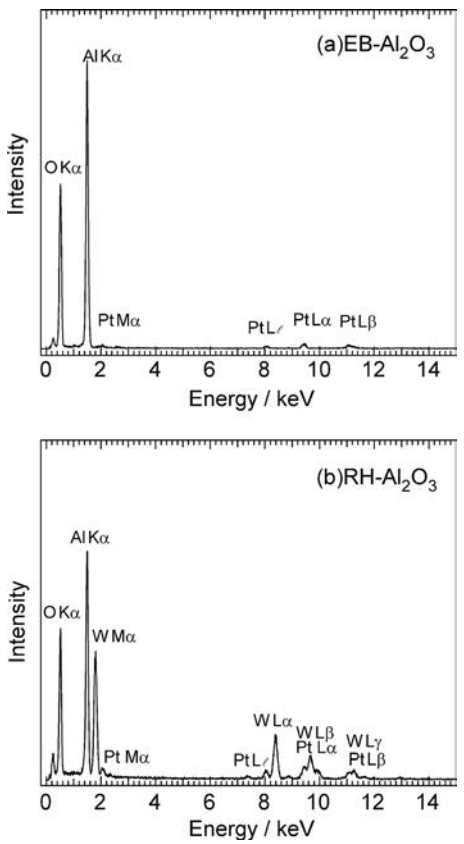

FIG. 1. EDS spectrum for as-deposited (a) EB-Al_2O_3 and (b) RH-Al_2O_3.

heating. The ratios of O/Al in EB-Al_2O_3 and O/(Al + W) in RH-Al_2O_3 were nearly 1.5.

A typical example of the changes in morphology and structure of amorphous EB-Al_2O_3 and RH-Al_2O_3 associated with annealing in air is shown in Fig. 2. No void contrast can be detected in an as-deposited thin film, as shown in the bright field images (BFIs) of Fig. 2(a). After annealing at 973 K for 3.6 ks (Fig. 2(b)), voids appear both in EB-Al_2O_3 and RH-Al_2O_3, as indicated by the bright contrast. The mean diameter of voids produced in EB-Al_2O_3 is 1.9 nm, while that in RH-Al_2O_3 is 3.3 nm. As shown in the corresponding SAED patterns in Figs. 2(a) and 2(b), the structure both before and after annealing at 973 K for 3.6 ks is amorphous. At 1073 K, crystallized regions appear in the amorphous matrix of EB-Al_2O_3, as has been reported by the authors.[4] The mean diameter of the nanovoids in the BFI of the crystallized region shown in Fig. 2(c) was estimated to be 2.6 nm. On the other hand, RH-Al_2O_3 fully crystallized at the same condition of 1073 K for 3.6 ks. It is noteworthy that the average void diameter is 6.9 nm, which is more than twice that of crystallized EB-Al_2O_3, and the maximum diameter is close to 10 nm. The Debye-Scherrer rings seen in Fig. 2(c) for EB-Al_2O_3 and RH-Al_2O_3 are consistently indexed as those of γ-Al_2O_3.

It has been reported that nanovoid formation in the crystallization process of amorphous Al_2O_3, which is approximately 20% less dense than γ-Al_2O_3, is most likely due to the accumulation of the large amount of free volume.[4] This is true of amorphous RH-Al_2O_3 with about 10 at. % W, because the formation and growth of nanovoids occur during the structural change toward γ-Al_2O_3 as it does in the case of EB-Al_2O_3 without W. However, there are clear differences in the crystallization and void formation behavior between EB-Al_2O_3 and RH-Al_2O_3. As shown in Fig. 2(c), RH-Al_2O_3 with W fully crystallized into γ-Al_2O_3 at 1073 K for 3.6 ks, while γ-Al_2O_3 appeared partly in the amorphous matrix of EB-Al_2O_3 without W[4], suggesting that crystallization in RH-Al_2O_3 is more rapid than in EB-Al_2O_3. This indicates that W atoms enhance the crystallization process in Al_2O_3, including nucleation and growth. In addition, the mean void diameter of 3.3 nm of amorphous RH-Al_2O_3 annealed at 973 K for 3.6 ks is not only larger than that of amorphous EB-Al_2O_3 annealed at 973 K for 3.6 ks, at 1.8 nm, but also larger than that of crystallized EB-Al_2O_3 annealed at 1073 K, at 2.6 nm. This clear enhancement of void formation, attributable to the inclusion of W atoms in RH-Al_2O_3, may be due to either kinetics or the structural differences between EB-Al_2O_3 and RH-Al_2O_3. The higher rate of nucleation and growth in RH-Al_2O_3 compared to EB-Al_2O_3 suggests that structural change toward crystallization is responsible for the enhancement of void formation. However, kinetics is unlikely to be the sole reason because even the mean void diameter of RH-Al_2O_3 in the amorphous states (3.3 nm, at 973 K) surpasses the diameter of fully crystallized EB-Al_2O_3 (3.0 nm, at 1123 K[4]). Accordingly, another factor, i.e., the structural change induced by W in Al_2O_3, should be taken into consideration.

Figure 3 shows atomic pair distribution functions (PDFs) for amorphous EB-Al_2O_3 and RH-Al_2O_3 obtained by analyzing the SAED patterns of amorphous regions. As shown in Fig. 3(a), Al-O, O-O, and Al-Al peaks can be seen at around 0.18, 0.28, and 0.32 nm, respectively, which is in good agreement with a number of experimental and simulated PDFs of amorphous and liquid Al_2O_3.[5,6,15–19] The PDFs for as-deposited and annealed EB-Al_2O_3 at 973 and 1073 K are almost consistent with respect to peak intensity and position.

In the case of RH-Al_2O_3 including W, the PDFs after annealing at 873 and 973 K are quite similar to those for EB-Al_2O_3 in terms of peak position, as shown in Fig. 3(b); the first and second peaks are located around 0.18 and 0.28 nm, respectively, although the position of the third peak is not clear. However, the PDF of the as-deposited amorphous RH-Al_2O_3 clearly differs from those of annealed amorphous RH-Al_2O_3. The major characteristics in the PDFs of RH-Al_2O_3 are (1) the first peak tends to increase and becomes sharper with increasing temperature and (2) the intensity of the second peak for the as-deposited amorphous state is larger than that for the annealed states. These characteristics suggest the amorphous structure of as-deposited RH-Al_2O_3 changes significantly as a result of annealing in air.

In Fig. 4, the PDF of as-deposited RH-Al_2O_3 is compared with that of as-deposited EB-Al_2O_3. It is evident that the first peak of RH-Al_2O_3 is much broader than EB-Al_2O_3 at larger r regions, indicating that additional correlation exists in RH-Al_2O_3, which includes a substantial amount of W atoms. The configuration of W-O bonds in amorphous WO_3 is heterogeneous; one is W^{+6}-O and the other is W^{+5}-O. The distribution of W-O bond length including W^{+6}-O

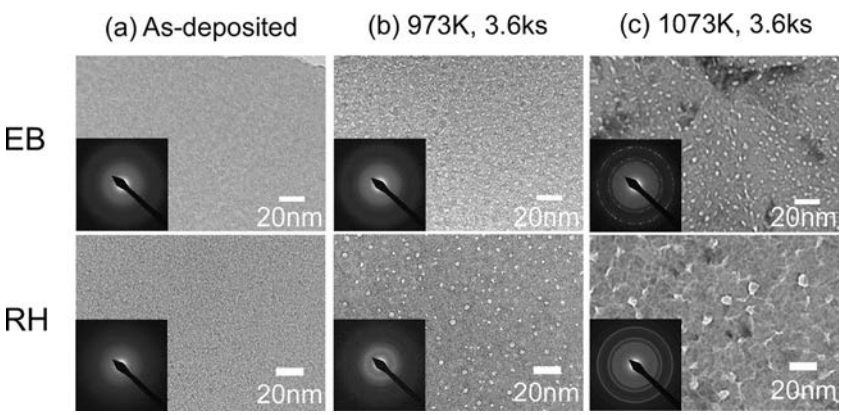

FIG. 2. BFIs and SAEDs of amorphous EB-Al_2O_3 and RH-Al_2O_3 before (a) and after annealing for 3.6 ks at (b) 973 K and (c) 1073 K. Reprinted with permission from R. Nakamura, T. Shudo, A. Hirata, M. Ishimaru, H. Nakajima, Scr. Mater., 64/2, 198 (2011). Copyright © 2011 Elsevier.

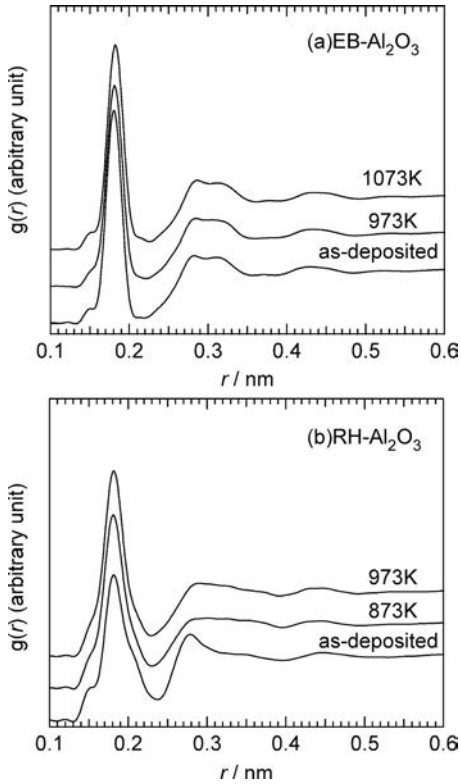

FIG. 3. PDFs of amorphous (a) EB-Al_2O_3 (as-deposited, 973 K, and 1073 K) and (b) RH-Al_2O_3 (as-deposited, 873 K, and 973 K).

and W^{+5}-O is known to be in the range between 0.14 and 0.24 nm,[20,21] which is in good agreement with the first minimum for as-deposited RH-Al_2O_3 located at 0.24 nm. Therefore, the broader distribution of the first peak is probably due to the existence of W-O bonds in RH-Al_2O_3. As shown in Fig. 3(b), moreover, the first peak at around 0.18 nm for as-deposited RH-Al_2O_3 becomes higher and sharper as the annealing temperature increases. This tendency suggests that the distribution of W-O bonds is close to that of Al-O because the long-range diffusion in the matrix results in drastic structural change.

It is not easy to establish the actual model of amorphous RH-Al_2O_3 including W by a calculation method, taking the structural change along with annealing into consideration. However, the MD simulations of amorphous and liquid Al_2O_3 with different densities provide some insight on the meaning of "heterogeneity" in terms of random structures. On the basis of the model developed by Tane *et al.*,[5] the atomistic structures of amorphous and liquid Al_2O_3 models were analyzed. The calculated PDFs of the amorphous Al_2O_3 model at 300 K (solid line), at 700 K (dotted line), and the liquid Al_2O_3 model at 2600 K (bold line) with a density of 3.34, 3.29, and 2.82 g/cm^3, respectively, are shown in Fig. 5. The PDFs of as-quenched and annealed amorphous Al_2O_3 reproduce those of EB-Al_2O_3 generated experimentally in terms of the peak positions demonstrated already by Tane *et al.*[5] The distribution of $g(r)$ for the Al-O peak of amorphous Al_2O_3 at 700 K tends to be somewhat broader than that of amorphous Al_2O_3 at 300 K with a lower density of 3.29 g/cm^3 as a result of the increase in lattice vibration. Compared to amorphous Al_2O_3, the amplitude of $g(r)$ for the Al-O peak of liquid Al_2O_3 with a density of 2.82 g/cm^3 falls off by approximately half and the distribution becomes even broader due to thermal lattice vibration in the liquid state. In the liquid Al_2O_3 model, AlO_2 and AlO_3 basic units are included in addition to AlO_4, AlO_5, and AlO_6, which are major basic units in amorphous Al_2O_3,[5,12,22] indicating that a variety of coordination causes a decrease in density and an increase in free volume. The PDF of amorphous RH-Al_2O_3 including W shown in Fig. 4 closely resembles that of liquid Al_2O_3. The similarity in the PDF of liquid Al_2O_3 and amorphous RH-Al_2O_3 may well be due to the structural change by W into amorphous Al_2O_3; the addition of W into amorphous Al_2O_3 brings about a structural change similar to the pseudo-liquid state, which is more heterogeneous at the atomistic scale and has lower density than the amorphous state.

In order to clarify the effect of W on the amorphous structure and the void formation behavior, HAADF-STEM was applied to the observation of the distribution of W in amorphous RH-Al_2O_3 because HAADF-STEM can provide useful information on the state of heavy atoms in matrices. Figure 6 shows the HAADF-STEM images of as-deposited and annealed (at 773 K for 3.6 ks) RH-Al_2O_3. For the HAADF-STEM imaging, a beam convergence of 10 mrad and a detector angle greater than 60 mrad were used. In Fig. 6(a), it is apparent that bright dots below 1 nm are

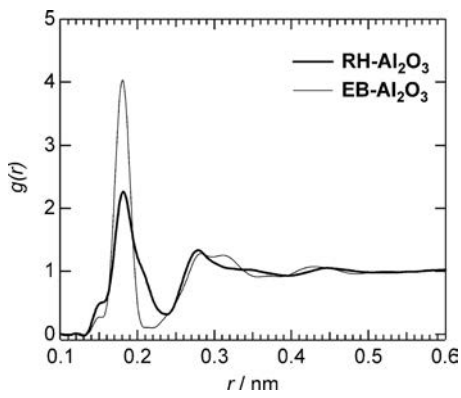

FIG. 4. Comparison of PDFs between as-deposited EB-Al_2O_3 and RH-Al_2O_3.

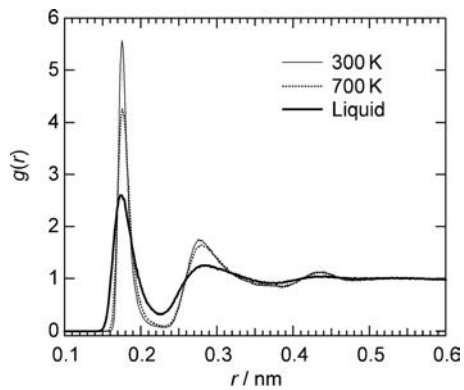

FIG. 5. MD simulations for PDFs of amorphous and liquid Al_2O_3. Solid line corresponds to amorphous Al_2O_3 model at 300 K with a density of 3.34 g/cm^3, dotted line to annealed amorphous Al_2O_3 model at 700 K with a density of 3.29 g/cm^3, and bold line to liquid Al_2O_3 model at 2600 K with a density of 2.82 g/cm^3.

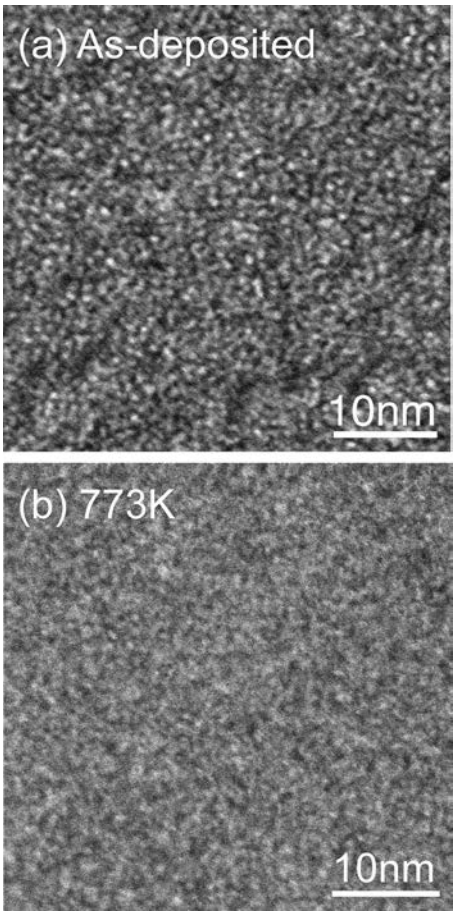

FIG. 6. HAADF-STEM images of (a) as-deposited and (b) 773 K-annealed RH-Al_2O_3.

homogeneously distributed in the matrix of as-deposited RH-Al_2O_3. It should be noted that the contrast becomes faint after annealing at 773 K in Fig. 6(b).

The contrast of HAADF-STEM images is known to be proportional to the square of the atomic number.[23] The thickness variation of the STEM specimens also gives rise to the contrast fluctuation in the image. To clarify the origin of the contrast in the HAADF image of Fig. 6(a), image simulations of the following atomistic models with a thickness of 12.3 nm were performed: (a) pure Al_2O_3 with a flat surface, (b) Al_2O_3 including a nano-pillar with a thickness of 12.3 nm, (c) Al_2O_3 including a W cluster with a diameter of 1.5 nm, and (d) Al_2O_3 with homogeneous W distribution (Fig. 7). It is not the amorphous structure itself that causes the strong contrast in the HAADF image (Fig. 7(a′)), but, the structural and compositional inhomogeneity of the specimens results in the contrast (Figs. 7(b′)–(d′)). In Fig. 7(b), an extreme model that has a nano-pillar height the same as the thickness of Al_2O_3 film was shown to have a weak contrast change (Fig. 7(b′)) compared to experimental results. The W clusters embedded in the Al_2O_3 matrix, however, were able to reproduce the features of Fig. 6(a), suggesting that the bright dots in Fig. 6(a) correspond to sub-nm sized W clusters. It should be noted that it is difficult to determine whether the clusters are composed merely by tungsten or by tungsten and oxygen. On the other hand, Fig. 7(d′) shows bright dots on the atomistic scale, which is in good agreement with the features of Fig. 6(b). On the basis of both the experimental and simulated results of the HAADF-STEM, the behavior of W atoms in the amorphous RH-Al_2O_3 matrix can be summarized as follows: W atoms are introduced in the form of sub-nm clusters by resistive heating deposition, and then have a tendency to dissolve into the amorphous matrix and react with oxygen atoms as a result of diffusion at elevated temperatures.

It was found in the PDF of as-deposited and annealed RH-Al_2O_3 shown in Fig. 3(b) that the first peak tends to increase and become sharper with increasing temperature and that the intensity of the second peak for the as-deposited amorphous state is larger than that of the annealed states. The change in the state of W observed by HAADF-STEM is in good agreement with the difference in PDF between as-deposited and annealed RH-Al_2O_3. The dissolution of W atoms into the amorphous matrix along with annealing induces the change in amorphous structure. For example, the increase in the first peak can be explained by the increase in the number of W-O bonds, resulting from the dissolution of W atoms into the Al-O matrix. While it is difficult to ascertain the origin of the change in the second peak for RH-Al_2O_3, it seems to be related to the formation of various W-related atomic bonds such as W-W and Al-W as a result of the dissolution of W atoms.

The PDF analysis revealed that RH-Al_2O_3 including W has a different structure from EB-Al_2O_3 without W. In other words, the introduction of W into amorphous Al_2O_3 causes heterogeneous atomic configurations characterized by a wide distribution of bond lengths, at around 0.18 nm at larger r regions in RH-Al_2O_3. The similarity between the PDF of amorphous RH-Al_2O_3 including W (Fig. 4) and that of liquid Al_2O_3 (Fig. 5) obtained by the MD simulation suggests that the addition of W into amorphous Al_2O_3 results in a structural change similar to a pseudo-liquid state, which is more disordered and has a larger free volume (lower density) than amorphous states.

According to extensive studies on the atomic configuration of amorphous Al_2O_3, it is commonly accepted that amorphous Al_2O_3 is composed of a majority of AlO_4 and AlO_5 basic units, and some AlO_6 units.[5,6,22] The introduction of W can disorder the state of coordination and bond-length in amorphous Al_2O_3. Because the valence of W^{5+} and W^{6+} is higher than that of Al^{3+}, W cations attract O^{2-} ions rather than Al cations, resulting in apparently poorer coordination of Al-O in amorphous Al_2O_3 including W. According to Wijs and Groot,[21] WO_6 and WO_5 are the majority and WO_7 and WO_4 are minority in amorphous WO_3. This indicates that the average coordination number of W-O is higher than that of Al-O, and implies of the existence of fewer coordinated O ions around Al in amorphous Al_2O_3 including W. The inhomogeneity in both coordination and bond-length in RH-Al_2O_3 promotes the irregularity of the unit structures, which means an excess free volume compared to amorphous Al_2O_3 without W. It is suggested that the increase in free volume due to the introduction of W serves to make these voids larger.

When samples are not homogeneous, a PDF analysis alone may give erroneous data due to sensitivity only to the

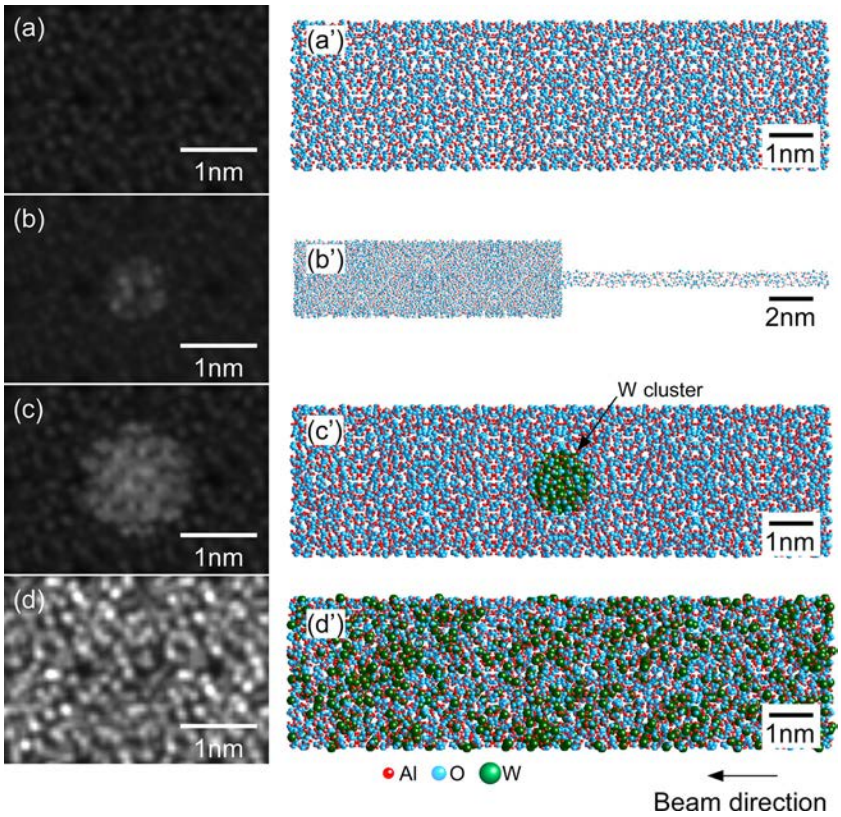

FIG. 7. (Color online) HAADF-STEM image simulations for amorphous Al_2O_3 with a thickness of 12.3 nm. (a) Pure amorphous Al_2O_3 with a flat surface, (b) amorphous Al_2O_3 with a nano-pillar of 12.3 nm thick, (c) amorphous Al_2O_3 in which W clusters with 1.5 nm are embedded, and (d) amorphous Al_2O_3 in which W atoms are homogeneously distributed. (a′)–(d′) show the corresponding atomic model.

nearest neighbor atomic distances. In such cases, it is necessary to observe the spatial distribution of atoms using imaging techniques. As mentioned earlier, the HAADF-STEM technique makes it possible to see the spatial distribution of heavy atoms directly in sub-nano scale. Owing to advances in TEM technologies, a simultaneous acquisition of PDFs and HAADF-STEM images is now available for identical thin films, which is a considerable improvement on the conventional diffraction techniques such as x-ray and neutron diffraction. As such, it is expected that the combination of the electron diffraction intensity PDF analysis and HAADF-STEM imaging will be increasingly used to analyze inhomogeneous and disordered states with dopant heavy atoms.

V. CONCLUSION

It was shown that W atoms played a role in the enhancement of the formation and growth of nanovoids in annealed amorphous Al_2O_3. The relationship between the enhancement of void formation and the amorphous structure was examined by a combination of PDF analysis and HAADF-STEM observations. The comparison of the PDFs of EB-Al_2O_3 without W and RH-Al_2O_3 with W revealed that heterogeneous atomic configuration was due to the introduction of W in amorphous Al_2O_3. Furthermore, the HAADF-STEM observations made it possible to describe the manner involving W in RH-Al_2O_3. The dissolution process of W atoms from sub-nm W clusters agrees well with the change in amorphous structure of RH-Al_2O_3 along with annealing. It is likely that the structural change in the amorphous structure induced by the addition of W brings about an increase in free volume, resulting in the increase in the void size in RH-Al_2O_3.

ACKNOWLEDGMENTS

TEM observations using H-800 and JEM-3000F were performed at the Research Center for Ultra-High Voltage Electron Microscopy and the Comprehensive Analysis Center of ISIR, Osaka University, respectively. This work was supported by Grant-in-Aid for Young Scientists (B) (No. 21760556) and also by Priority Assistance for the Formation of World Wide Renowned Centers of Research–The Global COE Program (Project: Center of Excellence for Advanced Structural and Functional Materials Design), from the Ministry of Education, Culture, Sports, Science and Technology, Japan.

[1]C. T. Kresge, M. E. Leonowicz, W. J. Roth, J. C. Vartuli, and J. S. Beck, Nature **359**, 710 (1992).
[2]S. A. Johnson, P. J. Ollivier, and T. E. Mallouk, Science **283**, 963 (1999).
[3]P. Yang, D. Zhao, D. I. Margolese, B. F. Chmelka, and G. D. Stucky, Nature **396**, 152 (1998).
[4]R. Nakamura, T. Shudo, A. Hirata, M. Ishimaru, and H. Nakajima, Scr. Mater. **64**, 197 (2011).
[5]M. Tane, S. Nakano, R. Nakamura, H. Ogi, M. Ishimaru, H. Kimizuka, and H. Nakajima, Acta Mater. **59**, 4631 (2011).
[6]G. Gutierrez and B. Johansson, Phys. Rev. B **65**, 104202 (2002).
[7]M. S. Mattson, Phys. Rev. B **58**, 11015 (1998).
[8]Y. Kimura and C. Kaito, J. Cryst. Growth **250**, 450 (2003).
[9]T. Ohkubo and Y. Hirotsu, Phys. Rev. B **67**, 094201 (2003).
[10]M. Ishimaru, I.-T. Bae, A. Hirata, Y. Hirotsu, J. A. Valdez, and K. E. Sickafus, Phys. Rev. B **72**, 024116 (2005).
[11]S. Nosé, Mol. Phys. **52**, 255 (1984); W. G. Hoover, Phys. Rev. A **31**, 1695 (1985).
[12]M. Parrinello and A. Rahman, J. Appl. Phys. **52**, 7182 (1981).

[13]M. Matsui, Miner. Mag. **58A**, 571 (1994).
[14]J. Lewis, D. Schwarzenbach, and H. D. Flack, Acta Crystal. A **38**, 733 (1982).
[15]P. Lamparter and R. Kniep, Physica B **234–236**, 405 (1997).
[16]M. A. S. Miguel, J. F. Sanz, L. J. Alvarez, and J. A. Odriozola, Phys. Rev. B **58**, 2369 (1998).
[17]S. P. Adiga, P. Zapol, and L. A. Curtiss, Phys. Rev. B **74**, 064204 (2006).
[18]S. Jahn and P. A. Madden, J. Non-Cryst. Solids **353**, 3500 (2007).
[19]P. Vashishta, R. K. Kalia, A. Nakano, and J. P. Rino, J. Appl. Phys. **103**, 083504 (2008).
[20]A. Kuzmin and J. Purans, J. Phys. Condens. Matter **5**, 2333 (1993).
[21]G. A. de Wijs and R. A. de Groot, Phys. Rev. B **60**, 16463 (1999).
[22]S. K. Lee, S. B. Lee, S. Y. Park, Y. S. Yi, and C. W. Ahn, Phys. Rev. Lett. **103**, 095501 (2009).
[23]N. D. Browning, M. F. Chisholm, and S. J. Pennycook, Nature **366**, 143 (1993).